International Journal of Solids and Structures 50 (2013) 2561–2572

Contents lists available at SciVerse ScienceDirect

International Journal of Solids and Structures

journal homepage: www.elsevier.com/locate/ijsolstr

Micro-to-macro transitions for continua with surface structure at the microscale

A. Javili [a,1], A. McBride [a,b,*], J. Mergheim [a,1], P. Steinmann [a,1], U. Schmidt [a,1]

[a] Chair of Applied Mechanics, University of Erlangen–Nuremberg, Egerlandstr. 5, 91058 Erlangen, Germany
[b] Centre for Research in Computational and Applied Mechanics, University of Cape Town, 5th floor Menzies Building, Private Bag X3, 7701 Rondebosch, South Africa

ARTICLE INFO

Article history:
Received 20 April 2012
Received in revised form 28 January 2013
Available online 11 April 2013

Keywords:
Homogenization
Surface elasticity
Size effects
Nanomaterials

ABSTRACT

A geometrically non-linear framework for micro-to-macro transitions is developed that accounts for the effect of size at the microscopic scale. This is done by endowing the surfaces of the microscopic features with their own (energetic) structure using the theory of surface elasticity. Following a standard first-order ansatz on the microscopic motion in terms of the macroscopic deformation gradient, a Hill-type averaging condition is used to link the two scales. The surface elasticity theory introduces two additional microscopic length scales: the ratio of the bulk volume to the energetic surface area, and the ratio of the surface and bulk Helmholtz energies. The influence of these microscopic length scales is elucidated via a series of numerical examples performed using the finite element method.

1. Introduction

The effective macroscopic properties of a heterogeneous material can be estimated from the response of the underlying microstructure using homogenisation procedures. These mature procedures need to be extended in certain situations (e.g. when the microstructure contains nanoscale voids) to account for the role of the surface at the microscale. A surface typically exhibits properties different from those of the bulk. These differences, caused by processes such as surface oxidation, ageing, coating, atomic rearrangement and the termination of atomic bonds, are present in comparatively thin boundary layers. Surface effects are especially significant for nanostructures due to their large surface-area-to-volume ratio. The objective of this contribution is to present a novel micro-to-macro transition (computational homogenisation) procedure that accounts for the role of the surface at the microscale. Possible applications would be a bulk material with nanoparticles or a nanoporous structure.

The two main ingredients of the work presented here are (i) continuum formulations that account for surface effects and (ii) homogenisation as pioneered by Hill (1963). A brief review of these topics is now given.

1.1. State-of-the-art review of continuum formulations which account for surfaces

Two of the key approaches used to study the thermodynamics of surfaces and interfaces are:

- the zero-thickness layer or Gibbs (geometrical) method wherein a mathematical surface with zero thickness is introduced to capture excess quantities on the surface (see e.g. Gibbs, 1961);
- the finite-thickness layer method, which dates back to the work of van der Waals in the late 19th century, wherein a layer of finite thickness is employed in place of the interface.

The methodology adopted in this work is based upon the first approach. The reader is referred to Guggenheim (1940) for further details and a comparison of these two approaches.

Following the approach of Gibbs (1961), various models have been proposed to endow the surface or interface with their own distinct properties (see e.g Adam, 1941; Shuttleworth, 1950; Herring, 1951; Orowan, 1970). A widely-adopted continuum model, proposed by Gurtin and Murdoch (1975, 1978), gives the surface its own tensorial stress measures (see e.g Cammarata, 1994; Dingreville and Qu, 2005; He and Lilley, 2008; Duan et al., 2009, for applications in nanomaterials). It is the Gurtin and Murdoch model of surface elasticity that underpins the work presented in this contribution.

Park et al. (2006, 2007) and Park and Klein (2008) developed an alternative continuum framework based on the surface Cauchy–Born model, an extension of the classical Cauchy–Born model to include surface stresses.

* Corresponding author at: Centre for Research in Computational and Applied Mechanics, University of Cape Town, 5th floor Menzies Building, Private Bag X3, 7701 Rondebosch, South Africa. Tel.: +27 (0) 21 650 3817; fax: +27 (0) 21 685 2281.
E-mail addresses: ali.javili@ltm.uni-erlangen.de (A. Javili), andrew.mcbride@uct.ac.za (A. McBride), julia.mergheim@ltm.uni-erlangen.de (J. Mergheim), paul.steinmann@ltm.uni-erlangen.de (P. Steinmann), ulrike.schmidt@ltm.uni-erlangen.de (U. Schmidt).
[1] Tel.: +49 (0) 9131 85 28502; fax: +49 (0) 9131 85 28503.

0020-7683/$ - see front matter © 2013 Elsevier Ltd. All rights reserved.
http://dx.doi.org/10.1016/j.ijsolstr.2013.03.022

The thermodynamic fundamentals of surface science were reviewed in Rusanov (1996, 2005). Müller and Saul (2004) presented a review on the importance of stress and strain effects on surface physics. The role of stress at solid surfaces was critically examined by Ibach (1997). Fischer et al. (2008) studied the role of surface energy and surface stress in phase-transforming nanoparticles and reported on the thermodynamics of a moving surface.

The effect of surface energetics for ellipsoidal inclusions and the size-dependent elastic state of embedded inhomogeneities was investigated by Sharma et al. (2003), Sharma and Ganti (2004) and Sharma and Wheeler (2007). They utilised the classical formulation of Eshelby (1951, 1957) for embedded inclusions and modified it by incorporating surface energies. Duan et al. (2005a) extended the Eshelby formalism for inclusion/inhomogeneity problems to the nanoscale. Effective mechanical and thermal properties of heterogeneous materials containing nano-inhomogeneities based on the generalised Eshelby formalism are investigated in Duan et al. (2005a,b) and Duan and Karihaloo (2007), see also related works (Benveniste and Miloh, 2001, Huang and Sun, 2007, Fischer and Svoboda, 2010, Mogilevskaya et al., 2008, Lim et al., 2006, He and Li, 2006, Mi and Kouris, 2006, Yvonnet et al., 2011).

Our own contributions include the development in Javili and Steinmann (2009, 2010a) of a novel finite-element framework for continua with energetic surfaces. The framework inherently accounts for geometrical nonlinearities and surface anisotropy. The theory of thermoelasticity at the nanoscale is elaborated upon in Javili and Steinmann (2010b, 2011). A unifying review of various approaches for accounting for surface, interface and curve energies was presented in Javili et al. (2013).

A novel aspect of the work presented here is the development of a *geometrically non-linear* homogenisation framework accounting for surface energies at the microscale. To the best of the authors' knowledge, neither the theoretical nor the numerical aspects of the present problem have been studied previously.

1.2. State-of-the-art review of homogenisation

Homogenisation, as pioneered by Hill (1963, 1972), provides a consistent methodology to link the macroscopic and microscopic scales and forms the basis for computational micro-to-macro transitions (Suquet, 1987; Guedes and Kikuchi, 1990; Terada and Kikuchi, 1995; Smit et al., 1998; Miehe et al., 1999; Michel et al., 1999; Feyel and Chaboche, 2000; Kouznetsova et al., 2001; Miehe, 2002; Miehe and Koch, 2002; Temizer and Wriggers, 2008). Motivated by the non-classical behaviour of continua at the nanoscale, the objective of this contribution is to present a novel computational micro-to-macro transition framework for problems where the microstructure possesses surface structure. Within this framework, the response of the macroscopic problem is governed by the standard model of finite elasticity. The constitutive response of a macroscopic material point is obtained from the (numerical) solution of a representative problem at the microscopic scale. The microscopic problem contains surfaces possessing their own energetic structure.[2]

The contribution of the energetic surface to the overall strength of the microscopic representative volume element (RVE) depends on two relative microscopic length scales. The first is the ratio of the volume of the RVE to the area of the energetic surface. The second is the ratio of the microscopic Helmholtz energies of the surface and the bulk.

[2] The label energetic denotes that the surface possesses mechanical and constitutive structures. These structures are independent to those of the bulk. For an extensive discussion on the choice of material parameters used to describe the surface and their relation to those in the bulk, the reader is referred to Javili et al. (2012b) and the references therein.

The macro- and microscopic problems satisfy the assumption of scale separation. Nonetheless, the microscale problem possesses two relative length scales. Thus, unlike the case where the microstructure contains no energetic surfaces, the magnitude of the relative length scales of the microscopic problem are important. The energetic surface structure allows one to capture the phenomenon whereby the strength of a specimen increases with decreasing size. Standard micro-to-macro transition frameworks, i.e. where the macro- and microstructures possess no enhanced continuum description, can not capture this strengthening effect. This phenomenon has been investigated numerically using surface elasticity theory (see e.g. Wei et al., 2006; Kaptay, 2005; Javili and Steinmann, 2009, 2010a), but not within a micro-to-macro transition framework as is done in this contribution.

Various alternative approaches have been proposed to capture size effects within a micro-to-macro transition framework. In the spirit of their pioneering work on capturing size effects using gradient plasticity formulations (see e.g. Mülhaus and Aifantis, 1991; Zbib and Aifantis, 1989) Zhu et al. (1997) used a unit-cell technique to model size effects in metal matrix composites. Van der Sluis et al. (1999) proposed a methodology to couple a micromorphic macroscopic description (see e.g. Eringen, 1999, for an extensive overview of micromorphic media) to an underlying classical continuum in order to describe heterogeneous polymers. Kouznetsova et al. (2002) developed a micro-to-macro transition framework that allows information on the higher-order kinematic fields to be transferred to a microstructure described by a classical continuum formulation. Geers et al. (2007) and Coenen et al. (2010) investigated the response of macroscopic thin sheets with heterogeneous microstructure using second-order computational homogenisation schemes (Geers et al., 2001; Kouznetsova et al., 2002; Geers et al., 2003; Kouznetsova et al., 2004). The macroscopic response is described by a fourth-order shell theory. A second-order computational homogenisation scheme is then required to transfer the higher-order macroscopic kinematics to the microscopic problem. The opposite approach was adopted by Hirschberger et al. (2008) for material layers with a micromorphic mesostructure. Further important contributions on the interpretation of micromorphic material using homogenisation and the homogenisation of micromorphic microstructures have been made by Forest (1998, 1999) and Forest et al. (2001). McBride et al. (2012) developed a model for the computational homogenisation of energetic macroscopic layers containing underlying microstruture.

The influence of an interphase surrounding an inclusion was recently investigated by Li et al. (2011) using a closed-form approach based upon the model proposed by Mori and Tanaka (1973). The results were compared against finite element computations where the interphase was explicitly accounted for. The influences of size, interphase thickness, and inclusion shape were all accurately predicted. The surface elasticity theory adopted here can predict the same type of behaviour. In related work, Brisard et al. (2010) determined the Hashin–Shtrikman bounds on the shear modulus of a nanocomposite containing spherical inclusions and also accounted for the interface effects. Micro-to-macro transitions for coupled consolidation problems in micro-heterogeneous porous media have recently been considered by Su et al. (2011). Here the pore pressure at the microscale plays an important role.

1.3. Structure of the manuscript

This manuscript is organised as follows. The notation and certain key concepts are briefly introduced. The standard finite elasticity formulation governing the response of the macrostructure is summarised in Section 2. Thereafter the response of the microstructure containing an energetic surface is given. The link

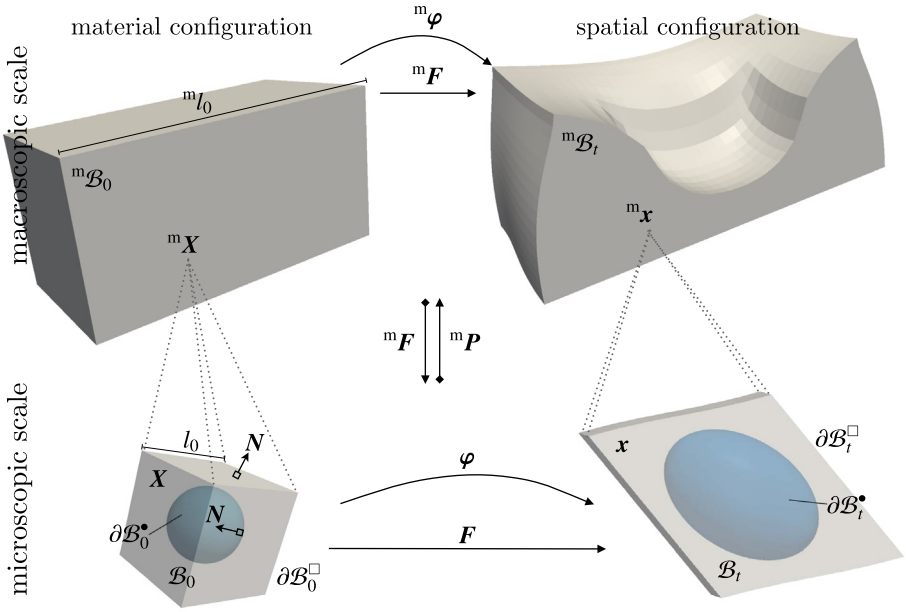

Fig. 1. A macroscopic domain $^{\mathrm{m}}\mathcal{B}_0$ possessing a surface with structure at the microscale. The domain $\mathcal{B}_0$ corresponds to a RVE. The motion $\boldsymbol{\varphi}$ of the microscopic RVE is associated with a macroscopic point $^{\mathrm{m}}\boldsymbol{X}$ within the bulk.

between the micro- and macro-problems is provided by the Hill-type averaging condition as discussed in Section 4. The theory is then elucidated via a series of numerical examples performed using the finite element method. In Section 6 we conclude and discuss various possible extensions to the work.

1.4. Notation

Direct notation is adopted throughout. Occasional use is made of index notation, the summation convention for repeated indices being implied. The scalar product of two vectors $\boldsymbol{a}$ and $\boldsymbol{b}$ is denoted $\boldsymbol{a}\cdot\boldsymbol{b}=[\boldsymbol{a}]_m[\boldsymbol{b}]_m$. The scalar product of two second-order tensors $\boldsymbol{A}$ and $\boldsymbol{B}$ is denoted $\boldsymbol{A}:\boldsymbol{B}=[\boldsymbol{A}]_{mn}[\boldsymbol{B}]_{mn}$. The composition of two second-order tensors $\boldsymbol{A}$ and $\boldsymbol{B}$, denoted $\boldsymbol{A}\cdot\boldsymbol{B}$, is a second-order tensor with components $[\boldsymbol{A}\cdot\boldsymbol{B}]_{ij}=[\boldsymbol{A}]_{im}[\boldsymbol{B}]_{mj}$. The action of a second-order tensor $\boldsymbol{A}$ on a vector $\boldsymbol{b}$ is a vector $\boldsymbol{c}=\boldsymbol{A}\cdot\boldsymbol{b}$ with components $[\boldsymbol{c}]_i=[\boldsymbol{A}]_{im}[\boldsymbol{b}]_m$. The tensor product of two vectors $\boldsymbol{a}$ and $\boldsymbol{b}$ is a second-order tensor $\boldsymbol{D}=\boldsymbol{a}\otimes\boldsymbol{b}$ with $[\boldsymbol{D}]_{ij}=[\boldsymbol{a}]_i[\boldsymbol{b}]_j$. A variable or operator defined at the macroscopic scale is distinguished from one at the microscopic scale via the left-superscript $^{\mathrm{m}}\{\bullet\}$. A microscopic variable or operator associated with the energetic surface is labelled as $\{\widehat{\bullet}\}$.

2. The macroscopic problem

Consider the macroscopic continuum body $^{\mathrm{m}}\mathcal{B}$ that takes the material configuration $^{\mathrm{m}}\mathcal{B}_0$ at time $t=0$, as shown in Fig. 1. The characteristic length associated with $^{\mathrm{m}}\mathcal{B}_0$ is denoted $^{\mathrm{m}}l_0$. A typical point within the material configuration is identified by the position vector $^{\mathrm{m}}\boldsymbol{X}$. The spatial configuration of the body at a later time is denoted $^{\mathrm{m}}\mathcal{B}_t$ with a typical point identified by the position vector $^{\mathrm{m}}\boldsymbol{x}$. The motion $^{\mathrm{m}}\boldsymbol{\varphi}$ relates the spatial and material placements as $^{\mathrm{m}}\boldsymbol{x}=^{\mathrm{m}}\boldsymbol{\varphi}(^{\mathrm{m}}\boldsymbol{X},t)$. The macroscopic, invertible linear tangent map $^{\mathrm{m}}\boldsymbol{F}$, i.e. the deformation gradient, is defined as the derivative of the macroscopic motion $^{\mathrm{m}}\boldsymbol{\varphi}$ with respect to the material configuration; that is,

$$^{\mathrm{m}}\boldsymbol{F}(^{\mathrm{m}}\boldsymbol{X},t):=\,^{\mathrm{m}}\mathrm{Grad}\,^{\mathrm{m}}\boldsymbol{\varphi}(^{\mathrm{m}}\boldsymbol{X},t), \tag{1}$$

where $^{\mathrm{m}}\mathrm{Grad}\{^{\mathrm{m}}\bullet\}:=\partial\{^{\mathrm{m}}\bullet\}/\partial\,^{\mathrm{m}}\boldsymbol{X}$.

The equation governing the macroscopic response (i.e. the strong form of the equilibrium equation), in the absence of body forces, is standard and given by

$$(^{\mathrm{m}}\mathrm{S})\quad\{\quad ^{\mathrm{m}}\mathrm{Div}\,^{\mathrm{m}}\boldsymbol{P}=\boldsymbol{0}, \tag{2}$$

where $^{\mathrm{m}}\boldsymbol{P}$ is the (macroscopic) Piola stress tensor. From the conservation of angular momentum one obtains the well-known relation

$$^{\mathrm{m}}\boldsymbol{F}\cdot\,^{\mathrm{m}}\boldsymbol{P}^t=\,^{\mathrm{m}}\boldsymbol{P}\cdot\,^{\mathrm{m}}\boldsymbol{F}^t. \tag{3}$$

The variational (weak) form of Eq. (2) follows as

$$\boxed{(^{\mathrm{m}}\mathrm{V})\quad\left\{\int_{^{\mathrm{m}}\mathcal{B}_0}{}^{\mathrm{m}}\boldsymbol{P}:\underbrace{^{\mathrm{m}}\mathrm{Grad}\delta\,^{\mathrm{m}}\boldsymbol{\varphi}}_{\delta\,^{\mathrm{m}}\boldsymbol{F}}\mathrm{d}V=\int_{\partial^{\mathrm{m}}\mathcal{B}_0^{\mathrm{N}}}\delta\,^{\mathrm{m}}\boldsymbol{\varphi}\cdot\,^{\mathrm{m}}\boldsymbol{T}^{\mathrm{p}}\mathrm{d}A,\right.} \tag{4}$$

for all admissible, arbitrary motions $\delta\,^{\mathrm{m}}\boldsymbol{\varphi}$. The part of the boundary of $^{\mathrm{m}}\mathcal{B}_0$ upon which the prescribed macroscopic Piola traction $^{\mathrm{m}}\boldsymbol{T}^{\mathrm{p}}$ acts is denoted $\partial^{\mathrm{m}}\mathcal{B}_0^{\mathrm{N}}$.

The left-hand side of Eq. (4) represents the total variational work of the macroscopic continuum. Accordingly, the variational work density at the macroscopic scale $\delta^{\mathrm{m}}\mathcal{W}_0$ is defined by

$$\delta^{\mathrm{m}}\mathcal{W}_0:=\,^{\mathrm{m}}\boldsymbol{P}:\delta^{\mathrm{m}}\boldsymbol{F}. \tag{5}$$

Relationship (5) identifies the macroscopic work conjugate kinetic and kinematic quantities as $^{\mathrm{m}}\boldsymbol{P}$ and $^{\mathrm{m}}\boldsymbol{F}$, respectively.

3. The microscopic problem

In accordance with the assumption of scale separation, a microscopic RVE of characteristic length $l_0\ll{}^{\mathrm{m}}l_0$ is associated with a macroscopic point at position $^{\mathrm{m}}\boldsymbol{X}$, as depicted in Fig. 1. The microscopic RVE takes the material configuration $\mathcal{V}_0$ with volume $|\,\mathcal{V}_0\,|$.

Consider an idealised microstructure composed of identical voids.[3] The RVE thus contains a void as indicated in Fig. 2(a). The bulk material surrounding the void is denoted $\mathcal{B}_0$. The boundary of the

[3] The framework presented here is not restricted to such idealised microstructures. The microstructure is chosen to elucidate the role of the surface contributions at the microscale.

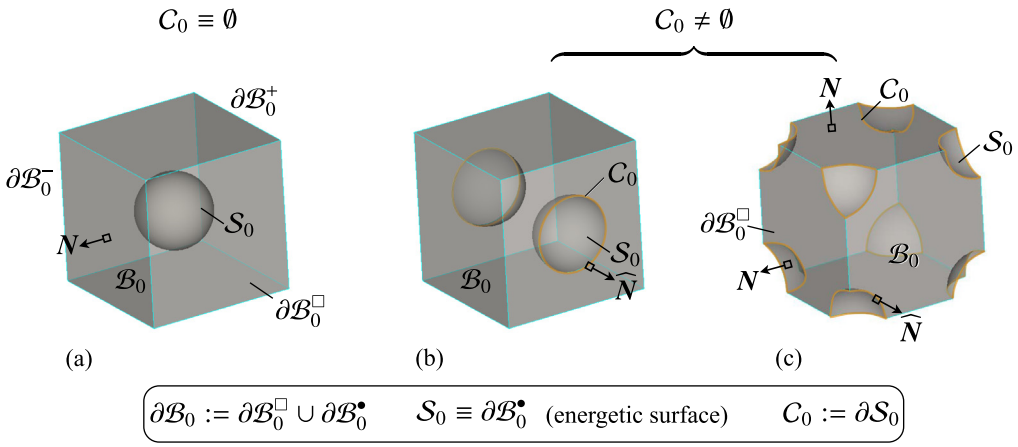

Fig. 2. Various possible RVEs for a periodic microstructure containing spherical voids.

bulk material can be decomposed into an exterior portion that coincides with the boundary of the RVE, denoted $\partial\mathcal{B}_0^\square$, and an interior portion that coincides with the surface of the void, denoted $\partial\mathcal{B}_0^\bullet$. Hence $\partial\mathcal{B}_0 = \partial\mathcal{B}_0^\square \cup \partial\mathcal{B}_0^\bullet$. In addition, the surface $\partial\mathcal{B}_0^\bullet$ is denoted $\mathcal{S}_0$ for the case where it is energetic. The RVEs shown in Fig. 2(b) and (c) are equivalent to the one shown in Fig. 2(a) but the boundary of the surface $\mathcal{C}_0 := \partial\mathcal{S}_0 \neq \emptyset$. For the sake of generality we assume throughout the subsequent derivation of the governing relationships that $\mathcal{C}_0 \neq \emptyset$.[4] The unit normal to the curve $\mathcal{C}_0$, tangent to $\mathcal{S}_0$, is denoted $\widehat{\boldsymbol{N}}$. The outward unit normal to $\partial\mathcal{B}_0$ is denoted $\boldsymbol{N}$.

A typical point within the material configuration is identified by the position vector $\boldsymbol{X}$. The spatial configuration of the body at a later time is denoted $\mathcal{B}_t$, with a typical point identified by the position vector $\boldsymbol{x}$. The motion $\boldsymbol{\varphi}$ relates the spatial and material placements as $\boldsymbol{x} = \boldsymbol{\varphi}(\boldsymbol{X}, t)$. The microscopic, invertible linear tangent map $\boldsymbol{F}$ is defined as the derivative of the microscopic motion $\boldsymbol{\varphi}$ with respect to the material configuration; that is,

$$\boldsymbol{F}(\boldsymbol{X}, t) := \mathrm{Grad}\,\boldsymbol{\varphi}(\boldsymbol{X}, t), \tag{6}$$

where $\mathrm{Grad}\{\bullet\} := \partial\{\bullet\}/\partial\boldsymbol{X}$. Furthermore, we assume from the onset that the surface is material, i.e. $\widehat{\boldsymbol{\varphi}} = \boldsymbol{\varphi}|_{\mathcal{S}_0}$.

We assume from the onset that the surface $\partial\mathcal{B}_0^\bullet$ (resp. $\mathcal{S}_0$) is subject to homogeneous external Neumann-type traction conditions. The microscopic boundary-value problem (i.e. the strong form) governing the response of the RVE, denoted (S), is given by (see Steinmann, 2008; Javili and Steinmann, 2010b, and the references therein for further details)

$$(\mathrm{S}) \quad \begin{cases} \mathrm{Div}\boldsymbol{P} = \boldsymbol{0} & \text{in } \mathcal{B}_0, \quad (7a) \\ \widehat{\mathrm{Div}}\widehat{\boldsymbol{P}} = \boldsymbol{P}\cdot\boldsymbol{N} & \text{on } \mathcal{S}_0, \quad (7b) \\ \boldsymbol{P}\cdot\boldsymbol{N} =: \boldsymbol{T} & \text{on } \partial\mathcal{B}_0^\square, \quad (7c) \\ \widehat{\boldsymbol{P}}\cdot\widehat{\boldsymbol{N}} =: \widehat{\boldsymbol{T}} & \text{on } \mathcal{C}_0, \quad (7d) \end{cases}$$

subject to admissible Dirichlet constraints on the motion. The Piola stress tensors in the bulk and on the surface are respectively given by the hyperelastic constitutive relations as

$$\boldsymbol{P} := \partial_{\boldsymbol{F}}\Psi(\boldsymbol{F}) \quad \text{and} \quad \widehat{\boldsymbol{P}} := \partial_{\widehat{\boldsymbol{F}}}\widehat{\Psi}(\widehat{\boldsymbol{F}}). \tag{8}$$

Furthermore, the surface stress $\widehat{\boldsymbol{P}}$ is a superficial second-order tensor Gurtin and Murdoch (1975) and thus possesses the property $\widehat{\boldsymbol{P}}\cdot\boldsymbol{N} = \boldsymbol{0}$. The Helmholtz energy functions in the bulk and on the surface are denoted Ψ and $\widehat{\Psi}$, respectively. The surface deformation gradient is defined by $\widehat{\boldsymbol{F}} := \mathrm{Grad}\,\widehat{\boldsymbol{\varphi}}\cdot\widehat{\boldsymbol{I}}$, where the material surface unit tensor is given by $\widehat{\boldsymbol{I}} := \boldsymbol{I} - \boldsymbol{N}\otimes\boldsymbol{N}$. The tensor $\boldsymbol{I}$ is the ordinary unit tensor in the material configuration. From the conservation of angular momentum on the surface one obtains the symmetry relation (cf. Eq. (3))

$$\widehat{\boldsymbol{F}}\cdot\widehat{\boldsymbol{P}}^t = \widehat{\boldsymbol{P}}\cdot\widehat{\boldsymbol{F}}^t. \tag{9}$$

The Piola tractions acting on the external boundary $\partial\mathcal{B}_0^\square$ and the boundary of the energetic surface $\mathcal{C}_0$ are denoted $\boldsymbol{T}$ and $\widehat{\boldsymbol{T}}$, respectively. The divergence operator on the surface is defined by $\widehat{\mathrm{Div}}\{\widehat{\bullet}\} := [\mathrm{Grad}\{\widehat{\bullet}\}\cdot\widehat{\boldsymbol{I}}] : \widehat{\boldsymbol{I}} = \widehat{\mathrm{Grad}}\{\widehat{\bullet}\} : \widehat{\boldsymbol{I}}$.

The variational form of the governing equation at the microscopic scale, denoted (V), is obtained as follows. Testing Eqs. (7a) and (7b) from the left with arbitrary motions $\delta\boldsymbol{\varphi}$ and $\delta\widehat{\boldsymbol{\varphi}} := \delta\boldsymbol{\varphi}|_{\mathcal{S}_0}$, respectively, integrating over the respective domains and then combining the results one obtains

$$\begin{aligned} 0 &= \int_{\mathcal{B}_0} \delta\boldsymbol{\varphi}\cdot\mathrm{Div}\boldsymbol{P}\,\mathrm{d}V + \int_{\mathcal{S}_0} \delta\widehat{\boldsymbol{\varphi}}\cdot[\widehat{\mathrm{Div}}\,\widehat{\boldsymbol{P}} - \boldsymbol{P}\cdot\boldsymbol{N}]\,\mathrm{d}A \\ &= \int_{\mathcal{B}_0} \Big[\mathrm{Div}(\delta\boldsymbol{\varphi}\cdot\boldsymbol{P}) - \boldsymbol{P} : \underbrace{\mathrm{Grad}\delta\boldsymbol{\varphi}}_{\delta\boldsymbol{F}}\Big]\,\mathrm{d}V \\ &\quad + \int_{\mathcal{S}_0} \Big[\mathrm{Div}\Big(\delta\widehat{\boldsymbol{\varphi}}\cdot\widehat{\boldsymbol{P}}\Big) - \widehat{\boldsymbol{P}} : \underbrace{\widehat{\mathrm{Grad}}\delta\widehat{\boldsymbol{\varphi}}}_{\delta\widehat{\boldsymbol{F}}} - \delta\widehat{\boldsymbol{\varphi}}\cdot\boldsymbol{P}\cdot\boldsymbol{N}\Big]\,\mathrm{d}A. \end{aligned}$$

In order to proceed we make use of the divergence theorems in the bulk and on the surface, respectively given by

$$\int_{\mathcal{B}_0} \mathrm{Div}\{\bullet\}\mathrm{d}V = \int_{\partial\mathcal{B}_0} \{\bullet\}\cdot\boldsymbol{N}\,\mathrm{d}A, \tag{10a}$$

$$\int_{\mathcal{S}_0} \widehat{\mathrm{Div}}\{\widehat{\bullet}\}\mathrm{d}A = \int_{\mathcal{C}_0} \{\widehat{\bullet}\}\cdot\widehat{\boldsymbol{N}}\,\mathrm{d}L - \int_{\mathcal{S}_0} \widehat{C}\{\widehat{\bullet}\}\cdot\boldsymbol{N}\,\mathrm{d}A, \tag{10b}$$

where $\widehat{C} := -\widehat{\mathrm{Div}}\boldsymbol{N}$ is twice the mean curvature of the surface. Using these relations and the superficial nature of the surface Piola stress, i.e. $\widehat{\boldsymbol{P}}\cdot\boldsymbol{N} = \boldsymbol{0}$, one obtains

[4] The surface $\mathcal{S}_0$ is assumed to be smooth. For the more general case where the surface $\mathcal{S}_0$ is non-smooth, the curve $\mathcal{C}_0$ can be understood as a geometrical entity. For the restricted case considered here, the curve $\mathcal{C}_0$ accounts for the interaction between the surface and the boundary of the RVE and should be understood as a physical entity. The extension of this work to non-smooth boundaries is straightforward. Nevertheless, it involves introducing additional geometric concepts and further notation while providing little additional insight into the fundamental concepts.

$$0=\int_{\partial\mathcal{B}_0}[\boldsymbol{P}\cdot\boldsymbol{N}]\cdot\delta\boldsymbol{\varphi}\,\mathrm{d}A-\int_{\mathcal{B}_0}\boldsymbol{P}:\delta\boldsymbol{F}\,\mathrm{d}V+\int_{\mathcal{C}_0}[\widehat{\boldsymbol{P}}\cdot\widehat{\boldsymbol{N}}]\cdot\delta\widehat{\boldsymbol{\varphi}}\,\mathrm{d}L$$
$$-\int_{\mathcal{S}_0}[\widehat{\boldsymbol{P}}:\delta\widehat{\boldsymbol{F}}+\delta\widehat{\boldsymbol{\varphi}}\cdot\boldsymbol{P}\cdot\boldsymbol{N}]\mathrm{d}A=\int_{\partial\mathcal{B}_0^{\square}}\underbrace{[\boldsymbol{P}\cdot\boldsymbol{N}]}_{\boldsymbol{T}}\cdot\delta\boldsymbol{\varphi}\,\mathrm{d}A$$
$$-\int_{\mathcal{B}_0}\boldsymbol{P}:\delta\boldsymbol{F}\,\mathrm{d}V+\int_{\mathcal{C}_0}\underbrace{[\widehat{\boldsymbol{P}}\cdot\widehat{\boldsymbol{N}}]}_{\widehat{\boldsymbol{T}}}\cdot\delta\widehat{\boldsymbol{\varphi}}\,\mathrm{d}L-\int_{\mathcal{S}_0}\widehat{\boldsymbol{P}}:\delta\widehat{\boldsymbol{F}}\,\mathrm{d}A.$$

Thus the variational form of the equation governing the microscopic response is given by

$$\boxed{(\mathrm{V})\Big\{\int_{\mathcal{B}_0}\boldsymbol{P}:\delta\boldsymbol{F}\mathrm{d}V+\int_{\mathcal{S}_0}\widehat{\boldsymbol{P}}:\delta\widehat{\boldsymbol{F}}\mathrm{d}A=\int_{\partial\mathcal{B}_0^{\square}}\boldsymbol{T}\cdot\delta\boldsymbol{\varphi}\mathrm{d}A+\int_{\mathcal{C}_0}\widehat{\boldsymbol{T}}\cdot\delta\widehat{\boldsymbol{\varphi}}\mathrm{d}L}\tag{11}$$

for all admissible, arbitrary motions $\delta\boldsymbol{\varphi}$ and $\delta\widehat{\boldsymbol{\varphi}}$. The total variational work associated with the microscopic problem is thus given by the left-hand side of Eq. (11).

4. Coupling the microscopic and macroscopic problems

The coupling between the microscopic and macroscopic problems is now described. Thereafter we discuss the issue of microscopic scale and the role it plays when the microstructure contains an energetic surface.

4.1. The Hill-type averaging condition

The celebrated Hill-type averaging condition (Hill, 1963, 1972) stipulates (variational) work equivalence between the macro- and microscopic scales. From the relations (5) at the macroscopic scale and (11) at the microscopic scale it follows that

$$\mathcal{H}:=\frac{1}{|\,\mathcal{V}_0\,|}\left[\int_{\mathcal{B}_0}\boldsymbol{P}:\delta\boldsymbol{F}\,\mathrm{d}V+\int_{\mathcal{S}_0}\widehat{\boldsymbol{P}}:\delta\widehat{\boldsymbol{F}}\mathrm{d}A\right]-\delta^{\mathrm{m}}\mathcal{W}_0\doteq 0.\tag{12}$$

The microscopic motion $\boldsymbol{\varphi}$ is linked to the macroscopic deformation by the standard first-order ansatz:

$$\boldsymbol{\varphi}(\boldsymbol{X},t)={}^{\mathrm{m}}\boldsymbol{F}(t)\cdot\boldsymbol{X}+\boldsymbol{w}(\boldsymbol{X},t),\tag{13}$$

where $\boldsymbol{w}(\boldsymbol{X},t)$ is the non-homogeneous fluctuation field. Thus,

$$\boldsymbol{F}=\mathrm{Grad}\boldsymbol{\varphi}={}^{\mathrm{m}}\boldsymbol{F}+\mathrm{Grad}\boldsymbol{w}.\tag{14}$$

The variations of the deformation gradients $\boldsymbol{F}$ and $\widehat{\boldsymbol{F}}$ follow as

$$\delta\boldsymbol{F}=\delta^{\mathrm{m}}\boldsymbol{F}+\mathrm{Grad}\delta\boldsymbol{w}\quad\text{and}\quad\delta\widehat{\boldsymbol{F}}=\delta\boldsymbol{F}\cdot\widehat{\boldsymbol{I}},\tag{15}$$

where, due to the coherency of the surface, $\delta\widehat{\boldsymbol{w}}=\delta\boldsymbol{w}|_{\mathcal{S}_0}$. Substituting Eq. (15) into Eq. (12) gives

$$0\doteq\mathcal{H}=\frac{1}{|\,\mathcal{V}_0\,|}\left[\int_{\mathcal{B}_0}\boldsymbol{P}:[\delta^{\mathrm{m}}\boldsymbol{F}+\mathrm{Grad}\delta\boldsymbol{w}]\mathrm{d}V+\int_{\mathcal{S}_0}\widehat{\boldsymbol{P}}:[\delta^{\mathrm{m}}\boldsymbol{F}\cdot\widehat{\boldsymbol{I}}+\widehat{\mathrm{Grad}}\delta\boldsymbol{w}]\mathrm{d}A\right]$$
$$-{}^{\mathrm{m}}\boldsymbol{P}:\delta^{\mathrm{m}}\boldsymbol{F}$$
$$=\left[\frac{1}{|\,\mathcal{V}_0\,|}\left[\int_{\mathcal{B}_0}\boldsymbol{P}\mathrm{d}V+\int_{\mathcal{S}_0}\widehat{\boldsymbol{P}}\mathrm{d}A\right]-{}^{\mathrm{m}}\boldsymbol{P}\right]:\delta^{\mathrm{m}}\boldsymbol{F}+\frac{1}{|\,\mathcal{V}_0\,|}\left[\int_{\mathcal{B}_0}\boldsymbol{P}:\mathrm{Grad}\delta\boldsymbol{w}\mathrm{d}V+\int_{\mathcal{S}_0}\widehat{\boldsymbol{P}}:\widehat{\mathrm{Grad}}\,\delta\boldsymbol{w}\mathrm{d}A\right],$$

$$\Rightarrow\quad\boxed{{}^{\mathrm{m}}\boldsymbol{P}=\frac{1}{|\,\mathcal{V}_0\,|}\left[\int_{\mathcal{B}_0}\boldsymbol{P}\mathrm{d}V+\int_{\mathcal{S}_0}\widehat{\boldsymbol{P}}\mathrm{d}A\right]}\tag{16}$$

and thus

$$0=\int_{\mathcal{B}_0}\boldsymbol{P}:\mathrm{Grad}\delta\boldsymbol{w}\mathrm{d}V+\int_{\mathcal{S}_0}\widehat{\boldsymbol{P}}:\widehat{\mathrm{Grad}}\,\delta\boldsymbol{w}\,\mathrm{d}A$$
$$=\int_{\mathcal{B}_0}[\mathrm{Div}(\delta\boldsymbol{w}\cdot\boldsymbol{P})-\delta\boldsymbol{w}\cdot\underbrace{\mathrm{Div}\boldsymbol{P}}_{\boldsymbol{0}}]\mathrm{d}V+\int_{\mathcal{S}_0}[\widehat{\mathrm{Div}}(\delta\boldsymbol{w}\cdot\widehat{\boldsymbol{P}})-\delta\boldsymbol{w}\cdot\underbrace{\widehat{\mathrm{Div}}\widehat{\boldsymbol{P}}}_{\boldsymbol{P}\cdot\boldsymbol{N}}]\mathrm{d}A$$

and using Eq. (10) and the superficiality of $\widehat{\boldsymbol{P}}$,

$$=\int_{\partial\mathcal{B}_0^{\square}}\delta\boldsymbol{w}\cdot\boldsymbol{T}\,\mathrm{d}A+\int_{\mathcal{C}_0}\delta\boldsymbol{w}\cdot\widehat{\boldsymbol{T}}\,\mathrm{d}L.\tag{17}$$

Somewhat remarkably, considering the non-standard nature of the Hill-type condition (12), Eq. (17) can be satisfied by imposing one of the following three standard constraints on the fluctuation field:

$$\text{(i)}\quad\underbrace{\delta\boldsymbol{w}=\boldsymbol{0}\text{ in }\mathcal{B}_0}_{\text{Taylor/Voigt}},\quad\text{(ii)}\quad\underbrace{\delta\boldsymbol{w}=\boldsymbol{0}\text{ on }\partial\mathcal{B}_0^{\square}\cup\mathcal{C}_0}_{\text{kinematic}},$$
$$\text{(iii)}\quad\underbrace{[\![\delta\boldsymbol{w}]\!]=\boldsymbol{0}\text{ on }\partial\mathcal{B}_0^{\square+}\cup\mathcal{C}_0^{+}}_{\text{periodic fluctuations}}.\tag{18}$$

Note, opposite faces of the boundary $\partial\mathcal{B}_0^{\square}$ and the curve $\mathcal{C}_0$ can be denoted as $\partial\mathcal{B}_0^{\square\pm}$ and $\mathcal{C}_0^{\pm}$, respectively, as shown in Fig. 2. The notation $[\![\{\bullet\}]\!]:=\{\bullet\}|_{\partial\mathcal{B}_0^{\square+}\cup\mathcal{C}_0^{+}}-\{\bullet\}|_{\partial\mathcal{B}_0^{\square-}\cup\mathcal{C}_0^{-}}$. If periodic fluctuations are chosen as specified in Eq. $(18)_3$, then the Hill-type averaging condition (12) is satisfied if the tractions $\boldsymbol{T}$ and $\widehat{\boldsymbol{T}}$ are anti-periodic.

From Eq. (16), the macroscopic Piola stress ${}^{\mathrm{m}}\boldsymbol{P}$ is obtained from the volume averaged contributions from the bulk and the energetic surface. Using Eq. (14) and (18), the macroscopic deformation gradient is simply the volume average of the microscopic deformation gradient in the bulk, i.e.

$${}^{\mathrm{m}}\boldsymbol{F}=\frac{1}{|\,\mathcal{V}_0\,|}\int_{\mathcal{B}_0}\boldsymbol{F}\,\mathrm{d}V.$$

Remark. Although the homogenised macroscopic Piola stress ${}^{\mathrm{m}}\boldsymbol{P}$ in Eq. (16) contains contributions from both the bulk and the energetic surface, it still possesses the standard symmetry property given in Eq. (3). This can be shown as follows. Consider the decomposition of the macroscopic deformation gradient into tangential (i.e. on the surface) and normal components as

$${}^{\mathrm{m}}\boldsymbol{F}={}^{\mathrm{m}}\boldsymbol{F}\cdot\underbrace{[\widehat{\boldsymbol{I}}+\boldsymbol{N}\otimes\boldsymbol{N}]}_{\boldsymbol{I}}={}^{\mathrm{m}}\widehat{\boldsymbol{F}}+{}^{\mathrm{m}}\widehat{\boldsymbol{F}}_{\perp}.$$

Thus using the superficiality properties of $\widehat{\boldsymbol{P}}$

$${}^{\mathrm{m}}\boldsymbol{F}\cdot\widehat{\boldsymbol{P}}^{t}={}^{\mathrm{m}}\widehat{\boldsymbol{F}}\cdot\widehat{\boldsymbol{P}}^{t}\quad\text{and}\quad\widehat{\boldsymbol{P}}\cdot{}^{\mathrm{m}}\boldsymbol{F}^{t}=\widehat{\boldsymbol{P}}\cdot{}^{\mathrm{m}}\widehat{\boldsymbol{F}}^{t}.$$

The symmetry of the homogenised macroscopic Piola stress ${}^{\mathrm{m}}\boldsymbol{P}$ in Eq. (16) then follows from the above relation in conjunction with Eq. (9) and Eq. (3).

4.2. Relative length scales in the microscopic problem

Classical theories of surface elasticity (Gurtin and Murdoch, 1975; Moeckel, 1975; Daher and Maugin, 1986; dell'Isola and Romano, 1987) do not assign a thickness to the surface. Hence, there is no *physical length scale*.[5] *Relative length scales* are present however. Consider the relation for the macroscopic Piola stress ${}^{\mathrm{m}}\boldsymbol{P}$ given in Eq. (16) expressed as follows:

$$\boxed{{}^{\mathrm{m}}\boldsymbol{P}=\frac{1}{|\,\mathcal{V}_0\,|}\int_{\mathcal{B}_0}\boldsymbol{P}\mathrm{d}V+\underbrace{\frac{|\,\mathcal{S}_0\,|}{|\,\mathcal{V}_0\,|}}_{1/l_0^{\square}}\frac{1}{|\,\mathcal{S}_0\,|}\int_{\mathcal{S}_0}\widehat{\boldsymbol{P}}\,\mathrm{d}A,}\tag{19}$$

where $|\,\mathcal{S}_0\,|$ is the area of $\mathcal{S}_0$. The presence of the term $l_0^{\square}$ [m] (the ratio of the solid volume to the energetic surface area) introduces a relative length scale. The greater the value of $1/l_0^{\square}$, the greater the influence of the energetic surface on the microscopic response

[5] Steigmann and Ogden (1999) introduced a physical length scale by incorporating flexural resistance into the theory of Gurtin and Murdoch (1975). Related works include those by Chhapadia et al. (2011) and Fried and Todres (2005).

and, in turn, on the macroscopic kinetic variable ${}^{\mathrm{m}}\boldsymbol{P}$. For the case of a cuboid RVE with volume l_0^3 containing a spherical inclusion of radius R, the ratio $1/l_0^{\square} \propto 1/R$.

It is also clear from Eq. (19) and the assumed hyperelastic constitutive response defined in Eq. (8) that the ratio $l_0^{\Psi} := \widehat{\Psi}/\Psi$ [m] introduces a second relative length scale.

The magnitude of the contribution from the energetic surface term in Eq. (19) can be changed by varying either $l_0^{\square}$ or l_0^{Ψ}, or both. It is also clear that equivalent results can be obtained by scaling either $1/l_0^{\square}$ or l_0^{Ψ} equally.

5. Numerical results

The theory developed in the previous sections is elucidated via a series of numerical examples in two and three space dimensions. The focus of this contribution is on determining the response of the microstructure assuming the macroscopic deformation gradient ${}^{\mathrm{m}}\boldsymbol{F}$ to be known. The numerical solution of the fully-coupled micro-to-macro problem is standard and is not discussed here. The microscopic response is approximated using a finite element formulation which accounts for the energetic surface (Javili and Steinmann, 2009, 2010a).

Periodic boundary conditions, i.e. the conditions described in Eq. $(18)_3$, are imposed on the microstructure. Bi- and triquadratic finite element interpolations are used.

5.1. Material models

The response of the microscopic bulk is governed by a hyperelastic neo-Hookean constitutive model, characterised by the Lamé parameters λ and μ, with a Helmholtz energy given by

$$\Psi(\boldsymbol{F}) = \frac{1}{2}\lambda \ln^2 J + \frac{1}{2}\mu[\boldsymbol{F}:\boldsymbol{F} - n^{\mathrm{dim}} - 2\ln J],$$

where $J := \mathrm{Det}\boldsymbol{F} > 0$ is the Jacobian determinant and n^{dim} is the number of space dimensions. Similarly, the neo-Hookean energetic surface is characterised by the surface Lamé parameters $\widehat{\lambda}$ and $\widehat{\mu}$ (see Javili and Steinmann, 2010b, for a detailed discussion on surface material parameters) and the surface Helmholtz energy is given by

$$\widehat{\Psi}(\widehat{\boldsymbol{F}}) = \frac{1}{2}\widehat{\lambda}\ln^2\widehat{J} + \frac{1}{2}\widehat{\mu}\left[\widehat{\boldsymbol{F}}:\widehat{\boldsymbol{F}} - [n^{\mathrm{dim}}-1] - 2\ln\widehat{J}\right], \tag{20}$$

where $\widehat{J} := \widehat{\mathrm{Det}}\,\widehat{\boldsymbol{F}} > 0$ is the surface Jacobian determinant (see e.g. Steinmann, 2008, for further details). Surface tension effects have been ignored in Eq. (20). For the two-dimensional theory $\widehat{\lambda} \equiv \widehat{\mu}$ (see Javili and Steinmann, 2009, for further information). The microscopic bulk Helmholtz energy Ψ is fixed for all two-dimensional examples by setting $\lambda = 12.1667$ [N/m^2] and $\mu = 8.0$ [N/m^2]. The surface properties are then varied. For the three-dimensional example $\lambda = 110744$ [N/m^2] and $\mu = 80193.8$ [N/m^2], and $\widehat{\lambda} = 55371.8$ [N/m] and $\widehat{\mu} = 40096.9$ [N/m].

5.2. Two-dimensional example: the influence of scale

Consider the two-dimensional RVE containing a void shown in Fig. 3. The surface of the void can be either energetic or standard. The RVE is subjected to three different macroscopic kinematic loading conditions obtained by specifying ${}^{\mathrm{m}}\boldsymbol{F}$. The conditions, denoted I–III, correspond to extension, simple shear and volumetric expansion, respectively.

As an integrity check on the numerical implementation we first consider the case where the surface is standard. The length scale $l_0^{\square} \equiv l_0^{\square\mathrm{ref}}$ is assigned to the RVE containing a single void (for a standard surface $l_0^{\square} \equiv |\,\mathcal{V}_0\,| \,/\, |\,\partial\mathcal{B}_0^{\bullet}\,|$). Note that $l_0^{\square\mathrm{ref}}$ is a fixed reference quantity. Neither increasing the number of elements used to mesh the domain containing the single void, nor increasing the ratio $l_0^{\square\mathrm{ref}}/l_0^{\square}$ (i.e. increasing the ratio of the surface area to bulk volume while keeping the volume $|\,\mathcal{V}_0\,|$ fixed) influenced the computed macroscopic Piola stress tensor ${}^{\mathrm{m}}\boldsymbol{P}$ significantly (see Table 1). This is to be expected. The microstructure is standard and thus possesses no length scale (physical or relative).

The surface of the void is now defined to be energetic. The reference material's surface Helmholtz energy is denoted $\widehat{\Psi}^{\mathrm{ref}}$. Consider first the case where the surface Helmholtz energy is fixed at $\widehat{\Psi}^{\mathrm{ref}}$ and the ratio $l_0^{\square\mathrm{ref}}/l_0^{\square}$ is increased. Increasing the ratio $l_0^{\square\mathrm{ref}}/l_0^{\square}$ alters the computed macroscopic stress ${}^{\mathrm{m}}\boldsymbol{P}$ for all three deformation modes as shown in Table 1. Near-identical results can be obtained by considering a domain containing only a single void and increasing the ratio $\widehat{\Psi}/\widehat{\Psi}^{\mathrm{ref}}$ (resp. l_0^{Ψ} as Ψ is fixed). That

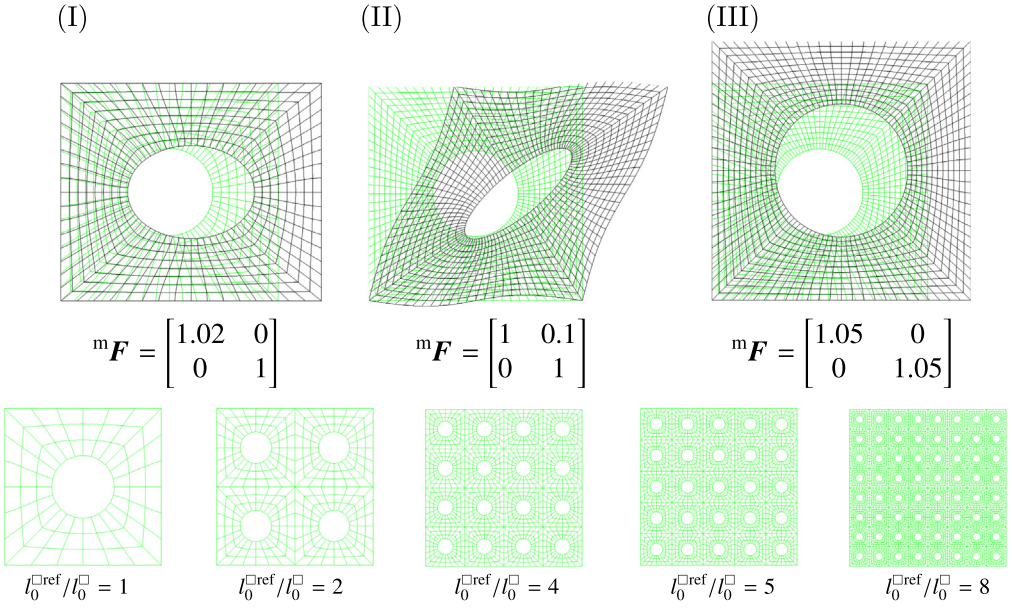

Fig. 3. The RVE and the loading conditions I–III corresponding to extension, simple shear and volumetric expansion, respectively. Also depicted are a range of possible RVEs and the associated length scale ratio $l_0^{\square\mathrm{ref}}/l_0^{\square}$.

Table 1
The homogenised macroscopic Piola stress ${}^{\mathrm{m}}\boldsymbol{P}$ obtained from a microstructure without and with an energetic surface. The results obtained by varying the ratio $l_0^{\square\mathrm{ref}}/l_0^{\square}$ and the inverse length scale l_0^{Ψ} are given.

	1	2	4	5	8
Standard surface					
$l_0^{\square\mathrm{ref}}/l_0^{\square}$					
I	$\begin{bmatrix} 3.81\times10^{-1} & -2.03\times10^{-8} \\ -1.99\times10^{-8} & 1.45\times10^{-1} \end{bmatrix}$	$\begin{bmatrix} 3.81\times10^{-1} & -2.03\times10^{-8} \\ -1.99\times10^{-8} & 1.45\times10^{-1} \end{bmatrix}$	$\begin{bmatrix} 3.81\times10^{-1} & -2.02\times10^{-8} \\ -1.98\times10^{-8} & 1.45\times10^{-1} \end{bmatrix}$	$\begin{bmatrix} 3.81\times10^{-1} & -2.00\times10^{-8} \\ -1.96\times10^{-8} & 1.45\times10^{-1} \end{bmatrix}$	$\begin{bmatrix} 3.81\times10^{-1} & -1.18\times10^{-5} \\ -1.14\times10^{-5} & 1.45\times10^{-1} \end{bmatrix}$
II	$\begin{bmatrix} 1.55\times10^{-2} & 5.37\times10^{-1} \\ 5.35\times10^{-1} & 2.18\times10^{-2} \end{bmatrix}$	$\begin{bmatrix} 1.55\times10^{-2} & 5.37\times10^{-1} \\ 5.35\times10^{-1} & 2.18\times10^{-2} \end{bmatrix}$	$\begin{bmatrix} 1.55\times10^{-2} & 5.37\times10^{-1} \\ 5.35\times10^{-1} & 2.18\times10^{-2} \end{bmatrix}$	$\begin{bmatrix} 1.55\times10^{-2} & 5.37\times10^{-1} \\ 5.35\times10^{-1} & 2.18\times10^{-2} \end{bmatrix}$	$\begin{bmatrix} 1.54\times10^{-2} & 5.37\times10^{-1} \\ 5.35\times10^{-1} & 2.17\times10^{-2} \end{bmatrix}$
III	$\begin{bmatrix} 1.26 & -1.17\times10^{-7} \\ -1.17\times10^{-7} & 1.26 \end{bmatrix}$	$\begin{bmatrix} 1.26 & -1.17\times10^{-7} \\ -1.17\times10^{-7} & 1.26 \end{bmatrix}$	$\begin{bmatrix} 1.26 & -1.17\times10^{-7} \\ -1.17\times10^{-7} & 1.26 \end{bmatrix}$	$\begin{bmatrix} 1.26 & -1.17\times10^{-7} \\ -1.17\times10^{-7} & 1.26 \end{bmatrix}$	$\begin{bmatrix} 1.26 & -5.05\times10^{-5} \\ -5.05\times10^{-5} & 1.26 \end{bmatrix}$
Energetic surface					
$l_0^{\square\mathrm{ref}}/l_0^{\square}$ where $l_0^{\Psi}\equiv l_0^{\Psi\,\mathrm{ref}}$					
I	$\begin{bmatrix} 5.81\times10^{-1} & -6.97\times10^{-9} \\ -6.83\times10^{-9} & 3.05\times10^{-1} \end{bmatrix}$	$\begin{bmatrix} 5.98\times10^{-1} & -8.64\times10^{-9} \\ -8.47\times10^{-9} & 3.20\times10^{-1} \end{bmatrix}$	$\begin{bmatrix} 6.07\times10^{-1} & -9.47\times10^{-9} \\ -9.28\times10^{-9} & 3.28\times10^{-1} \end{bmatrix}$	$\begin{bmatrix} 6.09\times10^{-1} & -9.64\times10^{-9} \\ -9.45\times10^{-9} & 3.30\times10^{-1} \end{bmatrix}$	$\begin{bmatrix} 6.12\times10^{-1} & -4.99\times10^{-6} \\ -4.96\times10^{-6} & 3.23\times10^{-1} \end{bmatrix}$
II	$\begin{bmatrix} 6.35\times10^{-2} & 6.80\times10^{-1} \\ 6.73\times10^{-1} & 6.53\times10^{-2} \end{bmatrix}$	$\begin{bmatrix} 6.86\times10^{-2} & 6.84\times10^{-1} \\ 6.77\times10^{-1} & 7.03\times10^{-2} \end{bmatrix}$	$\begin{bmatrix} 7.15\times10^{-2} & 6.87\times10^{-1} \\ 6.79\times10^{-1} & 7.31\times10^{-2} \end{bmatrix}$	$\begin{bmatrix} 7.21\times10^{-2} & 6.87\times10^{-1} \\ 6.80\times10^{-1} & 7.37\times10^{-2} \end{bmatrix}$	$\begin{bmatrix} 7.30\times10^{-2} & 6.88\times10^{-1} \\ 6.81\times10^{-1} & 7.46\times10^{-2} \end{bmatrix}$
III	$\begin{bmatrix} 2.12 & -1.15\times10^{-8} \\ -1.15\times10^{-8} & 2.12 \end{bmatrix}$	$\begin{bmatrix} 2.19 & -1.94\times10^{-8} \\ -1.94\times10^{-8} & 2.19 \end{bmatrix}$	$\begin{bmatrix} 2.22 & -2.30\times10^{-8} \\ -2.30\times10^{-8} & 2.22 \end{bmatrix}$	$\begin{bmatrix} 2.23 & -2.38\times10^{-8} \\ -2.30\times10^{-8} & 2.23 \end{bmatrix}$	$\begin{bmatrix} 2.24 & -1.13\times10^{-5} \\ -1.13\times10^{-5} & 2.24 \end{bmatrix}$
$l_0^{\Psi\mathrm{ref}}$ where $l_0^{\square}\equiv l_0^{\square\mathrm{ref}}$					
I	$\begin{bmatrix} 5.81\times10^{-1} & -6.97\times10^{-9} \\ -6.83\times10^{-9} & 3.05\times10^{-1} \end{bmatrix}$	$\begin{bmatrix} 5.98\times10^{-1} & -8.60\times10^{-9} \\ -8.43\times10^{-9} & 3.20\times10^{-1} \end{bmatrix}$	$\begin{bmatrix} 6.07\times10^{-1} & -9.59\times10^{-9} \\ -9.40\times10^{-9} & 3.28\times10^{-1} \end{bmatrix}$	$\begin{bmatrix} 6.09\times10^{-1} & -9.81\times10^{-9} \\ -9.61\times10^{-9} & 3.30\times10^{-1} \end{bmatrix}$	$\begin{bmatrix} 6.12\times10^{-1} & -1.01\times10^{-8} \\ -9.94\times10^{-9} & 3.23\times10^{-1} \end{bmatrix}$
II	$\begin{bmatrix} 6.35\times10^{-2} & 6.80\times10^{-1} \\ 6.73\times10^{-1} & 6.53\times10^{-2} \end{bmatrix}$	$\begin{bmatrix} 6.86\times10^{-2} & 6.84\times10^{-1} \\ 6.77\times10^{-1} & 7.03\times10^{-2} \end{bmatrix}$	$\begin{bmatrix} 7.15\times10^{-2} & 6.87\times10^{-1} \\ 6.79\times10^{-1} & 7.31\times10^{-2} \end{bmatrix}$	$\begin{bmatrix} 7.21\times10^{-2} & 6.87\times10^{-1} \\ 6.80\times10^{-1} & 7.37\times10^{-2} \end{bmatrix}$	$\begin{bmatrix} 7.30\times10^{-2} & 6.88\times10^{-1} \\ 6.81\times10^{-1} & 7.46\times10^{-2} \end{bmatrix}$
III	$\begin{bmatrix} 2.12 & -1.15\times10^{-8} \\ -1.15\times10^{-8} & 2.12 \end{bmatrix}$	$\begin{bmatrix} 2.19 & -1.86\times10^{-8} \\ -1.86\times10^{-8} & 2.19 \end{bmatrix}$	$\begin{bmatrix} 2.22 & -2.32\times10^{-8} \\ -2.32\times10^{-8} & 2.22 \end{bmatrix}$	$\begin{bmatrix} 2.23 & -2.42\times10^{-8} \\ -2.42\times10^{-8} & 2.23 \end{bmatrix}$	$\begin{bmatrix} 2.24 & -2.58\times10^{-5} \\ -2.58\times10^{-5} & 2.24 \end{bmatrix}$

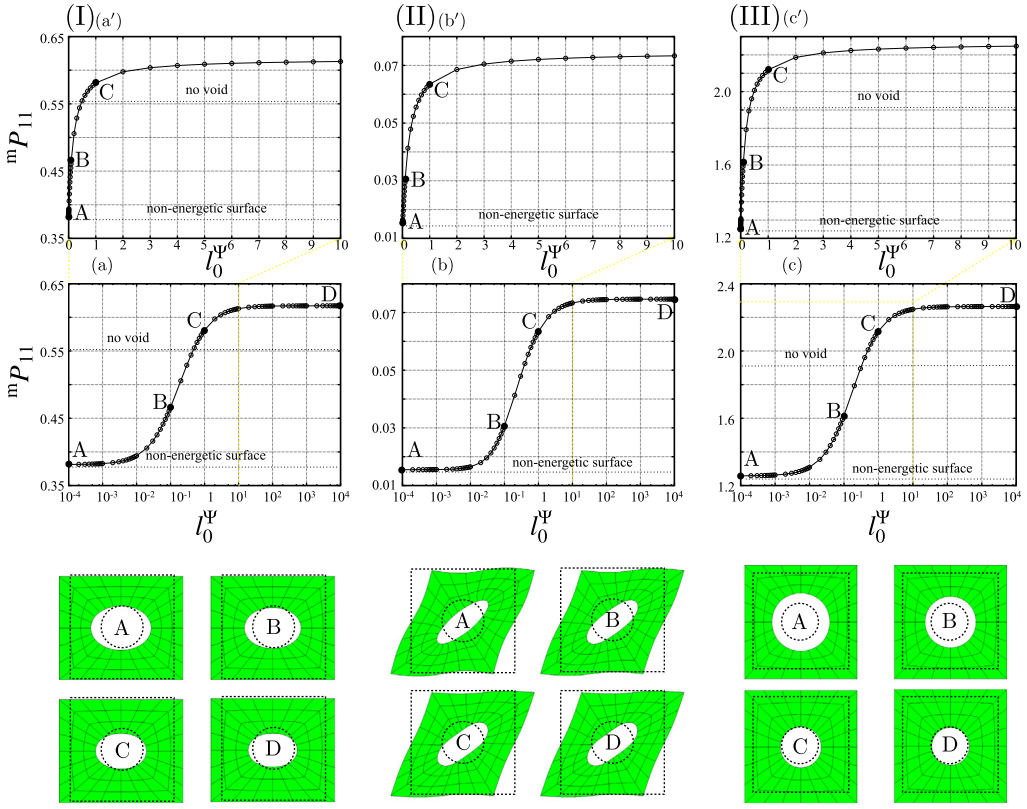

Fig. 4. The relationship between the macroscopic Piola stress component ${}^{\mathrm{m}}P_{11}$ and the length scale l_0^{Ψ} for the loading configurations I–III. The upper three graphs, labelled $(a'), (b'), (c')$, are the respective magnifications of those directly below, labelled (a), (b), (c). Also shown are the final deformed configurations corresponding to various values of l_0^{Ψ}.

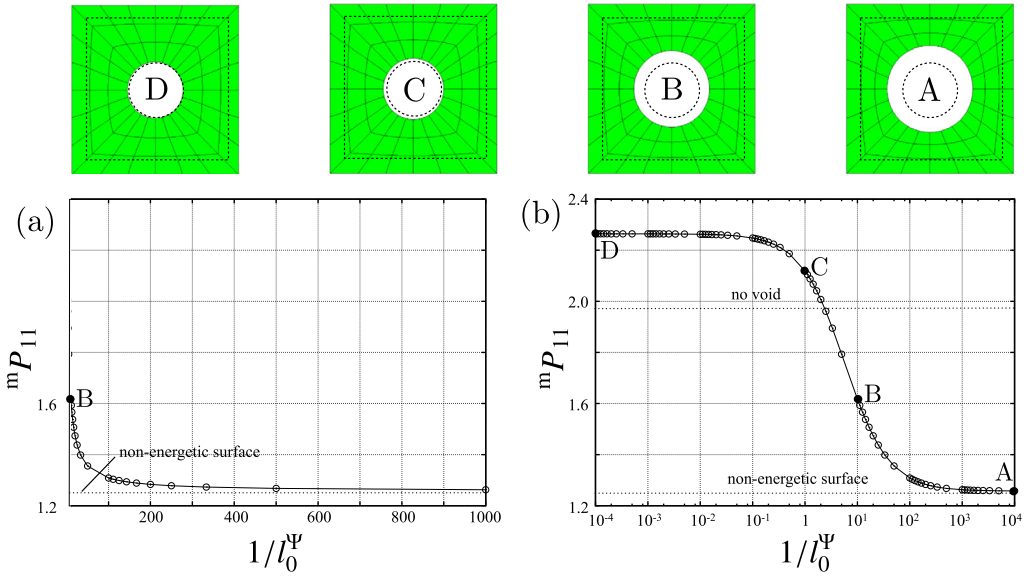

Fig. 5. The relationship between the homogenised macroscopic Piola stress component ${}^{\mathrm{m}}P_{11}$ and inverse length scale $1/l_0^{\Psi}$ for load case III.

this should be the case is clear from Eq. (19). The strength of the microstructure increases as the ratio $l_0^{\square\mathrm{ref}}/l_0^{\square}$ (resp. $\widehat{\Psi}/\widehat{\Psi}^{\mathrm{ref}}$ or l_0^{Ψ}) increases. As the resistance of the surface to the applied macroscopic deformation gradient ${}^{\mathrm{m}}\boldsymbol{F}$ increases relative to that of the bulk, so the bulk deforms to a greater extent. As demonstrated in Javili and Steinmann (2009), the energetic surface tries to preserve its initial surface area when subjected to loading. Increasing the length scale l_0^{Ψ} leads to a stiffer response of the surface. The direction of the surface normal $\boldsymbol{N}$ relative to the direction of applied loading also determines the ability of the surface to resist deformation.

It is also apparent from Table 1 that there is a limit to the additional strength that the energetic surface can confer upon the microstructure. This is more clearly seen from the results presented in Fig. 4. The ratio of the surface to bulk Lamé parameter $\widehat{\mu}/\mu = l_0^{\Psi}$ is varied in the range $(0, 10^4]$ and the macroscopic Piola

stress ${}^{\mathrm{m}}\boldsymbol{P}$ calculated. Note, a length scale of $l_0^{\Psi\mathrm{ref}} := l_0^{\Psi} \equiv 1$ corresponds to choosing $\widehat{\Psi} \equiv \widehat{\Psi}^{\mathrm{ref}}$. The standard problem without an energetic surface corresponds to $l_0^{\Psi} \equiv 0$. Choosing $l_0^{\Psi} \in (0, 0.01]$ gives the microstructure little additional strength. The resistance of the energetic surface to the applied deformation is less than the surrounding bulk. Thus the majority of the deformation is localised around the relatively weak void. A marked transition occurs when choosing $l_0^{\Psi} \in [0.01, 10]$. The energetic surface is now more able to resist the deformation than the surrounding bulk and the strength of the microstructure increases rapidly. The increase in strength with increasing l_0^{Ψ} reaches a limit at $l_0^{\Psi} \approx 10$. The response of the RVE without a void (also shown in Fig. 4) is weaker in some cases than that of the system with the void possessing an energetic surface.

In order to interpret these results consider the images in Fig. 4 showing the deformed domain superimposed upon the initial one. Increasing the surface Helmholtz energy increases the ability of the surface to maintain its initial area. This is most clearly seen for load case III as the macroscopic loading condition is purely volumetric. For the load cases I and II the response is more complex as the orientation of the surface relative to the loading varies along the surface and there is a Poisson effect from the bulk.

Material parameters for surface elasticity theory are often fitted from atomistic simulations (see e.g. Yvonnet et al., 2011). The suitably-averaged resistance of the atomistic system to an applied deformation can be related to a continuum stress measure. The domain of the atomistic simulation is then successively decreased to discern the role of the surface from that of the bulk. The discrete nature of an atomistic simulation imposes a physical size beyond which the domain can not be decreased. A continuum analogy to the atomistic fitting procedure can be obtained by decreasing the size of the microscopic domain, or equivalently, decreasing the inverse length scale $1/l_0^{\Psi}$. The results are shown in Fig. 5 for load case III. Due to the physical constraints limiting the smallest feasible size of an atomistic domain, one often sees atomistic fits that, qualitatively, resemble those presented in Fig. 5(a). The continuum domain can be decreased in size even further as shown in Fig. 5(b). It is now clear that the additional strengthening effect that comes with diminishing size reaches a limit (i.e. it saturates) for the reasons discussed when explaining the results in Fig. 4. The reader is referred to Forest et al. (2001) for a related discussion involving a micromorphic microstructure.

5.3. Two-dimensional example: the influence of shape

The shape and orientation of a void influence the strength of the RVE for a specific applied macroscopic loading. If the surface of the void is energetic, then the length scale l_0^{Ψ} also plays a role.

In order to investigate the role of shape, consider an elliptical void with its principal axes aligned with the basis vectors. The length of the horizontal and vertical principal axes are denoted a and b, respectively. The volume of the void is fixed and five different ratios of a/b are investigated for the three loading conditions depicted in Fig. 3. The area of the energetic surface is the same for $a/b = 1/4$ and $a/b = 4$, and $a/b = 4/9$ and $a/b = 9/4$, respectively. The results are given in Fig. 6.

The RVE becomes stronger as the inverse length scale $1/l_0^{\Psi}$ [m^{-1}] is decreased. For large values of $1/l_0^{\Psi}$ the results are as expected: the orientation and size of the void relative to the direction of loading determines the strength. As the value of $1/l_0^{\Psi}$ decreases so the energetic surface plays a more significant role. Consider the response corresponding to load case I shown in Fig. 6(a). For values of $1/l_0^{\Psi}$ greater than approximately 15, the responses for ratios $a/b = 4$ and $a/b = 9/4$ are indistinguishable. For values of $1/l_0^{\Psi}$ less than 15, the system containing the void with ratio $a/b = 4$ becomes stronger due to the larger amount of energetic surface area.

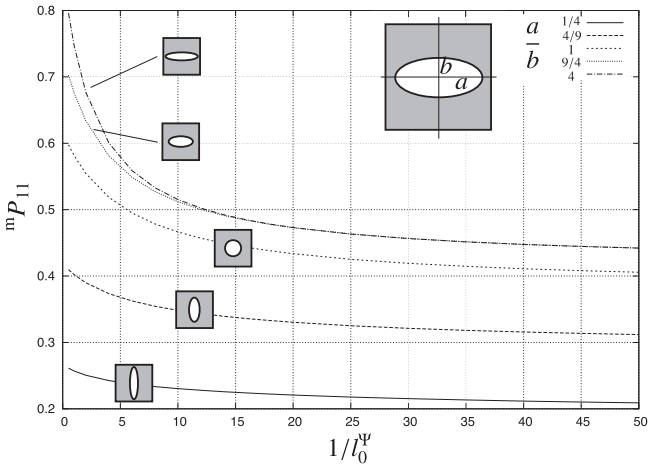

(a) Load case I.

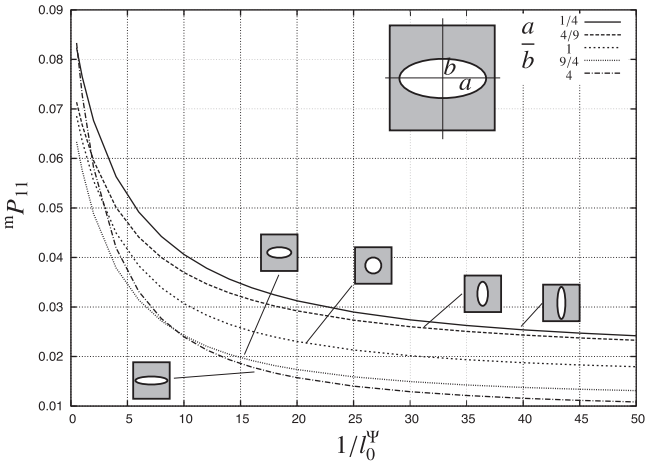

(b) Load case II.

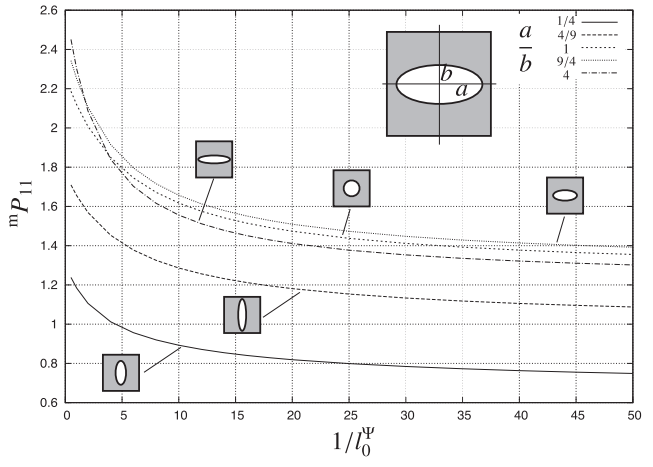

(c) Load case III.

Fig. 6. The influence of shape on the strength of the microstructure.

At small values of $1/l_0^{\Psi}$ the rate of gain of strength is greater for a ratio $a/b = 4$ than for $a/b = 1/4$ due to the alignment of the void relative to the load direction. Similar results are shown in Li et al. (2011) when modelling the influence of shape for an inclusion surrounded by an interphase.

More complex behaviour results when we consider load case II as shown in Fig. 6(b). The RVE containing a void with ratio $a/b = 1/4$

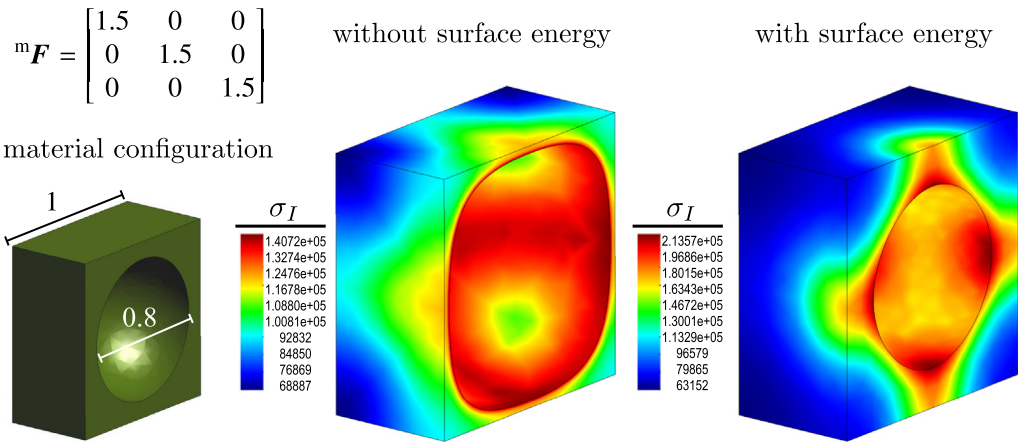

Fig. 7. The response of a three-dimensional microstructure to a macroscopic volumetric expansion type loading condition $^{m}\boldsymbol{F}$. The material and spatial configurations without and with an energetic surface are shown. The distribution of the von Mises stress $\boldsymbol{\sigma}_I$ [N/m^2] is indicated.

exhibits the strongest behaviour for large values of $1/l_0^{\Psi}$ while the ratio $a/b = 4$ exhibits the weakest (they both have the same surface area). For small values of $1/l_0^{\Psi}$ the RVE containing a void with ratio $a/b = 4$ increases in strength more rapidly than for $a/b = 1/4$. For small enough values of $1/l_0^{\Psi}$, $a/b = 4$ produces the strongest response.

5.4. Three-dimensional example

The response of a three-dimensional RVE to a volumetric expansion type macroscopic loading condition is shown in Fig. 7. The deformations are clearly large. The mechanical resistance of the energetic surface to the applied loading is clear. This additional resistance gives the RVE additional strength.

The volume average of the microscopic Piola stress in the absence of an energetic surface (i.e. the macroscopic Piola stress $^{m}\boldsymbol{P}$) is given by

$$\frac{1}{|\mathcal{V}_0|}\int_{\mathcal{B}_0} \boldsymbol{P}\,\mathrm{d}V = 7.563920 \times 10^4 \boldsymbol{I}.$$

Consider now the case where the energetic surface is present. The volume averages of the Piola stresses in the bulk and on the surface are respectively calculated as

$$\frac{1}{|\mathcal{V}_0|}\int_{\mathcal{B}_0} \boldsymbol{P}\,\mathrm{d}V = 1.252887 \times 10^5 \boldsymbol{I} \quad \text{and}$$
$$\frac{1}{|\mathcal{V}_0|}\int_{\mathcal{S}_0} \widehat{\boldsymbol{P}}\,\mathrm{d}A = 5.520450 \times 10^4 \boldsymbol{I}.$$

The contribution from the bulk alone is higher when the energetic surface is present. Furthermore, the surface adds additional strength over and above the bulk.

6. Discussion and conclusion

A micro-to-macro transition framework able to capture size effects at the microscale via the inclusion of energetic surfaces was presented. The dependence of the microscopic response, and in turn the homogenised macroscopic stress, on two relative microscopic length scales was made clear. A series of numerical examples elucidated the role of the relative length scales and the shape of the void.

One logical extension of this work is to implement the microstructural problem within a fully-coupled micro-to-macro scheme. This intended extension would be near identical to several contributions in the literature as the macroscopic response is standard (see e.g. Temizer and Wriggers, 2008, and references therein).

One obvious criticism of the surface elasticity theory used here is that the surface is a set of zero measure (i.e. it has no thickness) and hence has no physical length scale. The introduction of a physical length scale following the approach of Steigmann and Ogden (1999) will be pursued in future work. The recent work by Chhapadia et al. (2011) on curvature-dependent surface energies and the implications thereof for nanostructures will provide a good starting point. This extension will also overcome the pathological mesh dependence exhibited by models of surface elasticity that make use of negative material parameters fitted from atomistic calculations (see Javili et al., 2012b).

The material properties used in the two-dimensional example were chosen to qualitatively illustrate the response. Work is currently in progress to fit these material parameters from atomistic simulations for a range of actual materials. This would give further insight into the observed saturation effect.

The framework developed considered only a mechanical bulk and surface. The extension of the microscopic problem to account for thermal effects would follow directly from our contribution in Javili and Steinmann (2011). The micro-to-macro transition framework would have to be extended following the approaches developed in Ozdemir et al. (2008), Temizer and Wriggers (2011), for example.

Acknowledgements

The financial support of the German Science Foundation (Deutsche Forschungsgemeinschaft, DFG), Grant STE 544/39-1, is gratefully acknowledged. The support of the Cluster of Excellence "Engineering of Advanced Materials" at the University of Erlangen–Nuremberg, which is funded by the DFG within the framework of its "Excellence Initiative" is most appreciated. The second author thanks the National Research Foundation of South Africa for their support. The support of this work by the ERC Advanced Grant MOCOPOLY is gratefully acknowledged.

References

Adam, N.K., 1941. The Physics and Chemistry of Surfaces. Oxford University Press, London.
Benveniste, Y., Miloh, T., 2001. Imperfect soft and stiff interfaces in two-dimensional elasticity. Mechanics of Materials 33 (6), 309–323.
Brisard, S., Dormieux, L., Kondo, D., 2010. Hashin–Shtrikman bounds on the shear modulus of a nanocomposite with spherical inclusions and interface effects. Computational Materials Science 50 (2), 403–410.

Cammarata, R.C., 1994. Surface and interface stress effects in thin films. Progress in Surface Science 46 (1), 1–38.

Chhapadia, P., Mohammadi, P., Sharma, P., 2011. Curvature-dependent surface energy and implications for nanostructures. Journal of the Mechanics and Physics of Solids 59 (10), 2103–2115.

Coenen, E.W.C., Kouznetsova, V.G., Geers, M.G.D., 2010. Computational homogenization for heterogeneous thin sheets. International Journal for Numerical Methods in Engineering 83 (8–9), 1180–1205.

Daher, N., Maugin, G.A., 1986. The method of virtual power in continuum mechanics application to media presenting singular surfaces and interfaces. Acta Mechanica 60, 217–240.

dell'Isola, F., Romano, A., 1987. On the derivation of thermomechanical balance equations for continuous systems with a nonmaterial interface. International Journal of Engineering Science 25 (11–12), 1459–1468.

Dingreville, R., Qu, J., 2005. Surface free energy and its effect on the elastic behavior of nano-sized particles, wires and films. Journal of the Mechanics and Physics of Solids 53 (8), 1827–1854.

Duan, H.L., Karihaloo, B.L., 2007. Effective thermal conductivities of heterogeneous media containing multiple imperfectly bonded inclusions. Physical Review B 75, 064206.

Duan, H.L., Wang, J., Huang, Z.P., Karihalo, B.L., 2005a. Eshelby formalism for nano-inhomogeneities. Proceedings of the Royal Society A 461 (2062), 3335–3353.

Duan, H.L., Wang, J., Huang, Z.P., Karihaloo, B.L., 2005b. Size-dependent effective elastic constants of solids containing nano-inhomogeneities with interface stress. Journal of the Mechanics and Physics of Solids 53 (7), 1574–1596.

Duan, H.L., Wang, J., Karihaloo, B.L., 2009. Theory of elasticity at the nanoscale. Advances in Applied Mechanics 42, 1–68.

Eringen, A.C., 1999. Microcontinuum Field Theories I: Foundations and Solids. Springer, New York.

Eshelby, J.D., 1951. The force on an elastic singularity. Philosophical transactions of the Royal Society of London A 244, 87–112.

Eshelby, J.D., 1957. The determination of the elastic field of an ellipsoidal inclusion, and related problems. Proceedings of the Royal Society A 241 (1226), 376–396.

Feyel, F., Chaboche, J.-L., 2000. FE^2 multiscale approach for modelling the elastoviscoplastic behaviour of long fibre SiC/Ti composite materials. Computer Methods in Applied Mechanics and Engineering 183 (3–4), 309–330.

Fischer, F.D., Svoboda, J., 2010. Stresses in hollow nanoparticles. International Journal of Solids and Structures 47 (20), 2799–2805.

Fischer, F.D., Waitz, T., Vollath, D., Simha, N.K., 2008. On the role of surface energy and surface stress in phase-transforming nanoparticles. Progress in Materials Science 53 (3), 481–527.

Forest, S., 1998. Mechanics of generalized continua: construction by homogenization. Journal de Physique IV 8 (Pr4), 39–48.

Forest, S., 1999. Homogenization methods and the mechanics of generalized continua. Geometry, Continua and Microstructure. Hermann, Paris, pp. 35–48.

Forest, S., Pradel, F., Sab, K., 2001. Asymptotic analysis of heterogeneous cosserat media. International Journal of Solids and Structures 38 (26–27), 4585–4608.

Fried, E., Todres, R., 2005. Mind the gap: the shape of the free surface of a rubber-like material in proximity to a rigid contactor. Journal of Elasticity 80, 97–151.

Geers, M.G.D., Kouznetsova, V., Brekelmans, W.A.M., 2001. Gradient-enhanced computational homogenization for the micro–macro scale transition. Journal de Physique IV 11 (PR5), Pr5-145–Pr5-152.

Geers, M., Kouznetsova, V.G., Brekelmans, W.A.M., 2003. Multiscale first-order and second-order computational homogenization of microstructures towards continua. International Journal for Multiscale Computational Engineering 1 (4), 371–386.

Geers, M.G.D., Coenen, E.W.C., Kouznetsova, V.G., 2007. Multi-scale computational homogenization of structured thin sheets. Modelling and Simulation in Materials Science and Engineering 15 (4), S393.

Gibbs, J.W., 1961. The Scientific Papers of JW Gibbs, vol. 1. Dover Publications.

Guedes, J.-M., Kikuchi, N., 1990. Preprocessing and postprocessing for materials based on the homogenization method with adaptive finite element methods. Computer Methods in Applied Mechanics and Engineering 83 (2), 143–198.

Guggenheim, E.A., 1940. The thermodynamics of interfaces in systems of several components. Transactions of the Faraday Society 35, 397–412.

Gurtin, M.E., Murdoch, A.I., 1975. A continuum theory of elastic material surfaces. Archive of Rational Mechanics and Analysis 57, 291–323.

Gurtin, M.E., Murdoch, A.I., 1978. Surface stress in solids. International Journal of Solids and Structures 14 (6), 431–440.

He, L., Li, Z., 2006. Impact of surface stress on stress concentration. International Journal of Solids and Structures 43 (20), 6208–6219.

He, J., Lilley, C.M., 2008. Surface effect on the elastic behavior of static bending nanowires. Nano Letters 8 (7), 1798–1802.

Herring, C., 1951. Some theorems on the free energies of crystal surfaces. Physical Review 82 (1), 87–93.

Hill, R., 1963. Elastic properties of reinforced solids: some theoretical principles. Journal of the Mechanics and Physics of Solids 11, 357–372.

Hill, R., 1972. On constitutive macro-variables for heterogeneous solids at finite strain. Proceedings of the Royal Society of London A: Mathematical and Physical Sciences 326 (1565), 131–147.

Hirschberger, C.B., Sukumar, N., Steinmann, P., 2008. Computational homogenization of material layers with micromorphic mesostructure. Philosophical Magazine 88 (29), 3603–3631.

Huang, Z., Sun, L., 2007. Size-dependent effective properties of a heterogeneous material with interface energy effect: from finite deformation theory to infinitesimal strain analysis. Acta Mechanica 190, 151–163.

Ibach, H., 1997. The role of surface stress in reconstruction, epitaxial growth and stabilization of mesoscopic structures. Surface Science Reports 29 (5–6), 195–263.

Javili, A., Steinmann, P., 2009. A finite element framework for continua with boundary energies. Part I: The two-dimensional case. Computer Methods in Applied Mechanics and Engineering 198 (27–29), 2198–2208.

Javili, A., Steinmann, P., 2010a. A finite element framework for continua with boundary energies. Part I: The three-dimensional case. Computer Methods in Applied Mechanics and Engineering 199 (9–12), 755–765.

Javili, A., Steinmann, P., 2010b. On thermomechanical solids with boundary structures. International Journal of Solids and Structures 47 (24), 3245–3253.

Javili, A., Steinmann, P., 2011. A finite element framework for continua with boundary energies. Part III: The thermomechanical case. Computer Methods in Applied Mechanics and Engineering 200 (21–22), 1963–1977.

Javili, A., McBride, A., Steinmann, P., Reddy, B.D., 2012. Relationships between the admissible range of surface material parameters and stability of linearly elastic bodies. Philosophical Magazine 92 (28–30), 3540–3563.

Javili, A., McBride, A., Steinmann, P., 2013. Thermomechanics of solids with lower-dimensional energetics: on the importance of surface, interface and curve structures at the nanoscale. A unifying review. Applied Mechanics Reviews 65 (1), 010802.

Kaptay, G., 2005. Classification and general derivation of interfacial forces, acting on phases, situated in the bulk, or at the interface of other phases. Journal of Material Science 40, 2125–2131.

Kouznetsova, V., Brekelmans, W.A.M., Baaijens, F.P.T., 2001. An approach to micro–macro modeling of heterogeneous materials. Computational Mechanics 27, 37–84.

Kouznetsova, V., Geers, M.G.D., Brekelmans, W.A.M., 2002. Multi-scale constitutive modelling of heterogeneous materials with a gradient-enhanced computational homogenization scheme. International Journal for Numerical Methods in Engineering 54 (8), 1235–1260.

Kouznetsova, V.G., Geers, M.G.D., Brekelmans, W.A.M., 2004. Multi-scale second-order computational homogenization of multi-phase materials: a nested finite element solution strategy. Computer Methods in Applied Mechanics and Engineering 193 (48–51), 5525–5550.

Li, Y., Waas, A.M., Arruda, E.M., 2011. A closed-form, hierarchical, multi-interphase model for composites – derivation, verification and application to nanocomposites. Journal of the Mechanics and Physics of Solids 59 (1), 43–63.

Lim, C., Li, Z., He, L., 2006. Size dependent, non-uniform elastic field inside a nano-scale spherical inclusion due to interface stress. International Journal of Solids and Structures 43 (17), 5055–5065.

McBride, A.T., Mergheim, J., Javili, A., Steinmann, P., Bargmann, S., 2012. Micro-to-macro transitions for heterogeneous material layers accounting for in-plane stretch. Journal of the Mechanics and Physics of Solids 60 (6), 1221–1239.

Mi, C., Kouris, D.A., 2006. Nanoparticles under the influence of surface/interface elasticity. Journal of Mechanics of Materials and Structures 1 (4), 763–791.

Michel, J.C., Moulinec, H., Suquet, P., 1999. Effective properties of composite materials with periodic microstructure: a computational approach. Computer Methods in Applied Mechanics and Engineering 172 (1–4), 109–143.

Miehe, C., 2002. Strain-driven homogenization of inelastic microstructures and composites based on an incremental variational formulation. International Journal for Numerical Methods in Engineering 55, 1285–1322.

Miehe, C., Koch, A., 2002. Computational micro-to-macro transitions of discretized microstructures undergoing small strains. Archive of Applied Mechanics 72, 300–317.

Miehe, C., Schröder, J., Schotte, J., 1999. Computational homogenization analysis in finite plasticity. Simulation of texture development in polycrystalline materials. Computer Methods in Applied Mechanics and Engineering 171, 387–418.

Moeckel, G.P., 1975. Thermodynamics of an interface. Archive for Rational Mechanics and Analysis 57, 255–280.

Mogilevskaya, S.G., Crouch, S.L., Stolarski, H.K., 2008. Multiple interacting circular nano-inhomogeneities with surface/interface effects. Journal of the Mechanics and Physics of Solids 56 (6), 2298–2327.

Mori, T., Tanaka, K., 1973. Average stress in matrix and average elastic energy of materials with misfitting inclusions. Acta Metallurgica 21 (5), 571–574.

Mülhaus, H.-B., Aifantis, E.C., 1991. A variational principle for gradient plasticity. International Journal of Solids and Structures 28 (7), 845–857.

Müller, P., Saul, A., 2004. Elastic effects on surface physics. Surface Science Reports 54 (5–8), 157–258.

Orowan, E., 1970. Surface energy and surface tension in solids and liquids. Proceedings of the Royal Society A 316 (1527), 473–491.

Ozdemir, I., Brekelmans, W.A.M., Geers, M.G.D., 2008. FE^2 computational homogenization for the thermo-mechanical analysis of heterogeneous solids. Computer Methods in Applied Mechanics and Engineering 198, 602–613.

Park, H.S., Klein, P.A., 2007. Surface Cauchy–Born analysis of surface stress effects on metallic nanowires. Physical Review B 75 (8), 1–9.

Park, H.S., Klein, P.A., 2008. A surface Cauchy–Born model for silicon nanostructures. Computer Methods in Applied Mechanics and Engineering 197 (41–42), 3249–3260.

Park, H.S., Klein, P.A., Wagner, G.J., 2006. A surface Cauchy–Born model for nanoscale materials. International Journal for Numerical Methods in Engineering 68 (10), 1072–1095.

Rusanov, A.I., 1996. Thermodynamics of solid surfaces. Surface Science Reports 23, 173–247.

Rusanov, A.I., 2005. Surface thermodynamics revisited. Surface Science Reports 58, 11–239.

Sharma, P., Ganti, S., 2004. Size-dependent eshelby's tensor for embedded nano-inclusions incorporating surface/interface energies. Journal of Applied Mechanics 71, 663–671.

Sharma, P., Wheeler, L.T., 2007. Size-dependent elastic state of ellipsoidal nano-inclusions incorporating surface/interface tension. Journal of Applied Mechanics 74 (3), 447–454.

Sharma, P., Ganti, S., Bhate, N., 2003. Effect of surfaces on the size-dependent elastic state of nano-inhomogeneities. Applied Physics Letters 82 (4), 535–537.

Shuttleworth, R., 1950. The surface tension of solids. Proceedings of the Physical Society Section A 63 (5), 444–457.

Smit, R.J.M., Brekelmans, W.A.M., Meijer, H.E.H., 1998. Prediction of the mechanical behavior of nonlinear heterogeneous systems by multi-level finite element modeling. Computer Methods in Applied Mechanics and Engineering 155, 181–192.

Steigmann, D.J., Ogden, R.W., 1999. Elastic surface–substrate interactions. Proceedings: Mathematical, Physical and Engineering Sciences 455 (1982), 437–474.

Steinmann, P., 2008. On boundary potential energies in deformational and configurational mechanics. Journal of the Mechanics and Physics of Solids 56, 772–800.

Su, F., Larsson, F., Runesson, K., 2011. Computational homogenization of coupled consolidation problems in micro-heterogeneous porous media. International Journal for Numerical Methods in Engineering 88 (11), 1198–1218.

Suquet, P.M., 1987. Elements of homogenization of inelastic solid mechanics. In: Sanchez-Palencia, E., Zaoui, A. (Eds.), Homogenization Techniques for Composite Media. Springer-Verlag, Berlin, pp. 193–278.

Temizer, I., Wriggers, P., 2008. On the computation of the macroscopic tangent for multiscale volumetric homogenization problems. Computer Methods in Applied Mechanics and Engineering 198, 195–210.

Temizer, I., Wriggers, P., 2011. Homogenization in finite thermoelasticity. Journal of the Mechanics and Physics of Solids 59 (2), 344–372.

Terada, K., Kikuchi, N., 1995. Nonlinear homogenization method for practical applications. In: Ghosh, S., Ostoja-Starzewski, M. (Eds.), Computational Methods in Micromechanics, vol. AMD-212/MD-62. ASME, pp. 1–16.

van der Sluis, O., Vosbeek, P.H.J., Schreurs, P.J.G., Meijer, H.E.H., 1999. Homogenization of heterogeneous polymers. International Journal of Solids and Structures 36 (21), 3193–3214.

Wei, G., Shouwen, Y., Ganyun, H., 2006. Finite element characterization of the size-dependent mechanical behaviour in nanosystems. Nanotechnology 17 (4), 1118–1122.

Yvonnet, J., Mitrushchenkov, A., Chambaud, G., He, Q.-C., 2011. Finite element model of ionic nanowires with size-dependent mechanical properties determined by ab initio calculations. Computer Methods in Applied Mechanics and Engineering 200 (5–8), 614–625.

Zbib, H.M., Aifantis, E.C., 1989. A gradient-dependent flow theory of plasticity: application to metal and soil instabilities. Applied Mechanics Reviews 42 (11), S295–S304.

Zhu, H.T., Zbib, H.M., Aifantis, E.C., 1997. Strain gradients and continuum modeling of size effect in metal matrix composites. Acta Mechanica 121, 165–176.